Remote Sensing of Environment 269 (2022) 112829

Contents lists available at ScienceDirect

Remote Sensing of Environment

journal homepage: www.elsevier.com/locate/rse

Continuous monitoring of forest change dynamics with satellite time series

Mathieu Decuyper [a,b,*], Roberto O. Chávez [c], Madelon Lohbeck [a,b], José A. Lastra [c], Nandika Tsendbazar [b], Julia Hackländer [b], Martin Herold [b,d], Tor-G Vågen [a]

[a] World Agroforestry, Nairobi, Kenya
[b] Wageningen University & Research, Laboratory of Geo-Information Science and Remote Sensing, Droevendaalsesteeg 3, 6708 PB Wageningen, the Netherlands
[c] Laboratorio de Geo-Información y Percepción Remota, Instituto de Geografía, Pontificia Universidad Católica de Valparaíso, Valparaíso, Chile
[d] Helmholtz GFZ German Research Centre for Geosciences, Section 1.4 Remote Sensing and Geoinformatics, Telegrafenberg, Potsdam, 14473, Germany

ARTICLE INFO

Editor: Marie Weiss

Keywords:
Forest change detection
Continuous
Landsat
Secondary forest
Restoration
AVOCADO

ABSTRACT

Several forest change detection algorithms are available for tracking and quantifying deforestation based on dense Landsat and Sentinel time series satellite data. Only few also capture regrowth after clearing in an accurate and continuous way across a diversity of forest types (including dry and seasonal forests) and are thus suitable to address the need for better information on secondary forest succession and for assessing forest restoration activities. We present a new change detection algorithm that makes use of the flexibility of kernel density estimations to create a forest reference phenology, taking into account all historical phenological variations of the forest rather than smoothing these out by curve fitting. The AVOCADO (**A**nomaly **V**egetati**o**n **Ch**a**n**ge **D**etecti**o**n) algorithm allows detection of anomalies with a spatially explicit likelihood measure. We demonstrate the flexibility of the algorithm for three contrasting sites using all available Landsat time series data; ranging from tropical rainforest to dry miombo forest ecosystems, with different time series data densities, and characterized by different forest change types (e.g. selective logging, shifting cultivation). We found that the approach produced in general high overall accuracies (> 90%) across these varying conditions, but had lower accuracies in the dry forest site with a slight overestimation of disturbances and regrowth. The latter was due to the similarity of crops in the time series NDMI signal, causing false regrowth detections. In the moist forest site the low producer accuracies in the intact forest and regrowth class was due to its very small area class (most forest disappeared by the nineties). We showed that the algorithm is capable of capturing small-scale (gradual) changes (e.g. selective logging, forest edge logging) and the multiple changes associated to shifting cultivation. The performance of the algorithm has been shown at regional scale, but if larger scale studies are required a representative selection of reference forest types need to be selected carefully. The outputs of the change maps allow the estimation of the spatio-temporal trends in the proportions of intact forest, secondary forest and non-forest - information that is useful for assessing the areas and potential of secondary forests to accumulate carbon and forest restoration targets. The algorithm can be used for disturbance and regrowth monitoring in different ecozones, is user friendly, and open source.

1. Introduction

Forests are home to many of the world's species and play a vital role in providing key services to humanity. Currently most of the world's remaining tropical forest is degraded or secondary forest located inside human-modified landscapes (FAO, 2010). To understand the role that forests play now and in the future we need to understand the dynamics of changes in forested areas, including both disturbance and deforestation as well as processes of regrowth and secondary succession. The role of secondary succession in achieving restoration targets is increasingly recognized (Chazdon and Guariguata, 2016). Restoration based on natural regeneration is less costly and more effective than those based on tree planting (Chazdon and Uriarte, 2016; Crouzeilles et al., 2017). Naturally regenerated secondary forests are resilient, store large amounts of carbon (Chazdon et al., 2016; Cook-Patton et al., 2020; Poorter et al., 2016) and host many tree species (Rozendaal et al., 2019). However, the benefits for restoration depend on how long these forests persist, or the permanence of new forest growth. Previous studies on

* Corresponding author at: World Agroforestry, Nairobi, Kenya.
E-mail address: mathieu.decuyper@wur.nl (M. Decuyper).

https://doi.org/10.1016/j.rse.2021.112829
Received 7 February 2021; Received in revised form 8 October 2021; Accepted 26 November 2021
Available online 13 December 2021

secondary succession in Mexico have shown that age is the most important predictor of recovery of secondary forest diversity (Lohbeck et al., 2012), and of biomass and other essential functions (Lohbeck et al., 2015). Secondary forests are often part of a shifting cultivation land use system. Here secondary forests are the fallows that are used to recover soil conditions before it is cleared again for crop production. In such systems secondary forests persist for short periods only, limiting their contribution to conservation and restoration, as was demonstrated in the Brazilian Amazon where median persistence is about five years (Jakovac et al., 2017). Studies in Mexico showed a median persistence of seven years (Lohbeck et al., 2021), while in Costa Rica it has been shown to be 20 years (Reid et al., 2019), significantly increasing their role in conservation and restoration compared to studies with shorter fallow periods. In order to make use of natural regeneration for restoration there is a great need to understand how long secondary forests persist. However, long term historical field data from plots are scarce and data based on interviews can be unreliable and difficult to obtain. Remote sensing based on historical records, that are now increasingly available, plays an important role in quantifying and understanding past forest dynamics.

Remote sensing is now widely recognized as an invaluable tool for monitoring forest change, for instance through Global Forest Watch (Hansen et al., 2013). Having almost 50 years of data, Landsat is probably the most used satellite dataset for time series analysis. With the opening of the Landsat archive, forest change detection methods have rapidly developed over the last decade, allowing more comprehensive forest monitoring (Kennedy et al., 2014; Wulder et al., 2012). Before this time, forest change detection mapping was done using bi-temporal differences or supervised image classifications (Coppin et al., 2004). While these techniques were able to detect deforestation, they are less suitable for assessing small scale deforestation and regrowth as they do not capture the dynamic behavior of vegetation during the year and over longer time-periods. More recent change detection algorithms make use of cloud free images to create annual composites (Griffiths et al., 2014; Hansen et al., 2013; Huang et al., 2010; Kennedy et al., 2010, Kennedy et al., 2012). While these approaches have been shown to produce high accuracies for abrupt disturbances (e.g. slash and burn or clear-cut practices), studies that use all available data to create a dense time series demonstrated its potential in also detecting small scale forest disturbances and gradual changes (DeVries et al., 2015b; Verbesselt et al., 2010, 2012; Zhu et al., 2012; Zhu and Woodcock, 2014), and regrowth (DeVries et al., 2015a; Hamunyela et al., 2020). In addition, using all available data can be of large importance in areas with a strong seasonality where change detection methods using annual composites or (partially) smoothing out the seasonal variation yield low accuracies (Bos et al., 2019). In general, such new methods are promising in smallholder agricultural landscapes, that are characterized by complex forest dynamics caused by shifting cultivation, forest degradation and large variety of agroecosystems (Mananze et al., 2020). However, demonstrated methods on change monitoring are usually limited to one disturbance and one follow-up regrowth detection, while typically this is a continuous process, for example in areas where shifting cultivation is practiced. This has been tackled by methods using temporal segmentation and trend analysis (Dutrieux et al., 2016). Nevertheless, these methods rely on parametric functions to capture the undisturbed forest condition, or the normal phenological annual cycle of vegetation, and thus heavily rely on the quality of the fit. Usually, this is a function with an explicit seasonal component, for example, sine or cosine functions (Anees et al., 2013; Anees and Aryal, 2014; Zhu and Woodcock, 2014), double logistic functions (Olsson et al., 2016) or harmonic functions (Pasquarella et al., 2017; Verbesselt et al., 2010). These functions assume that regular, annual waves are a good representation of the plant phenological cycle, which is not always the case, especially in semi-arid and arid ecosystems (Broich et al., 2015; Chávez et al., 2019b). Approaches using parametric functions are the most used in current literature (de Beurs and Henebry, 2010; Shimizu et al., 2019). An alternative approximation of the annual phenological baseline, and one that we build on in this paper, is to use the observed frequency values, and define the expected distribution directly from observed data without reference to a theoretical model (Chávez et al., 2019c). The advantage of this approach is its flexibility to adapt to the particular conditions of every site and also to account for natural variability in annual phenology over time (which is smoothed over by the parametric functions). This approach is based on probabilistic estimations of the annual phenology, from which disturbances measured as anomalies from the expected phenology can be assessed in terms of the frequency distribution of historical records, providing both a map showing the likelihood of the change detection and the change detection result itself. Current methods based on parametric functions lack such a likelihood measure.

In this study we present and test a new algorithm which we coin, "AVOCADO" (**A**nomaly **V**egetati**o**n **Ch**a**n**ge **D**etecti**o**n). It is based on the R package "npphen" (Chávez et al., 2017; Estay and Chávez, 2018), developed to monitor phenology changes, and adjusted to monitor forest disturbance and regrowth in a semi-automated and continuous way. The algorithm uses all available data and does not require certain pre-processing steps such as removing outliers. The reference vegetation (undisturbed forest in this case) is taken from nearby pixels that are known to be undisturbed during the whole time series, so there is no need to set aside part of the time series as an historical baseline, which is usually taken at the beginning of the time series when incomplete data can lead to commission or omission errors. By using the complete time series in AVOCADO, more accurate predictions of vegetation changes can be made while improving the ability to deal with temporal gaps in the satellite data. Forest monitoring using this method is continuous, so it has the ability to detect multiple forest to non-forest transitions and vice versa. Furthermore, the algorithm accounts for the natural variability of the annual phenology, which makes it potentially more suitable to monitor areas with strong seasonality and gradual/small changes (such as degradation and forest regrowth).

To test the performance of AVOCADO with respect to the nature of the changes (e.g. selective logging, shifting agriculture) and different forest ecosystems, we selected three sites in three different ecological zones (i.e. a classification of the broad forest types based on climate criteria) (FAO, 2012) ranging from (1) tropical rainforest (Madre de Dios - Peru), to (2) tropical moist deciduous forest (Genteguela - Ivory Coast), and (3) tropical dry forest (Kilosa - Tanzania). The sites also differ in the types of changes that occur. In Madre de Dios the changes are often large-scale slash and burn and intermediate-scale shifting agriculture, while the changes in Genteguela and Kilosa are often small-scale selective logging and gradual forest disturbances. The aim of this study is to map forest disturbance and regrowth in a continuous way and test AVOCADO's robustness for detecting disturbance and regrowth at different spatial scales, characterized by abrupt and gradual changes and for systems experiencing different seasonality.

2. Material and methods

2.1. The AVOCADO algorithm

The continuous forest disturbance and regrowth monitoring AVOCADO algorithm is based on the "npphen" R package, which makes use of the flexibility of kernel density estimations to account for the annual phenological behavior of vegetation and its variability (Chávez et al., 2017; Estay and Chávez, 2018). The kernel density estimation in the vegetation index time-space works by centering a bivariate kernel (e.g. a Gaussian kernel) around each observation, and by averaging the heights of all kernels until obtaining the final density estimation. For more details about theoretical aspects of kernel density estimation see Wand and Jones (1994). By using the kernel density estimations the algorithm accounts for the phenological variations that occur in a satellite image pixel, rather than smoothing these out by fitting a parametric model over a subset of the time series. The kernel density estimations give the

position of each anomalous value within the frequency distribution of the observed values at a given date (e.g. a negative anomaly outside the 95% of the reference frequency distribution, hereafter referred to as RDF). This means that a RDF $\geq$ 0.95, indicates that the detected anomaly belongs to the lowest values recorded in the time series. Notice that anomalous values belonging to the remaining 5% of the frequency distribution can be located at the two extremes of the distribution, i.e. negative anomalies correspond to the 2.5% of the lowest values of the frequency distribution. Current methods lack such a likelihood measure. This kind of probabilistic approach has been successfully used to assess different types of vegetation disturbance, including wildfires (Bowman et al., 2019), insect outbreaks (Chávez et al., 2019c; Estay et al., 2019; Gutiérrez et al., 2020), climate extremes (Decuyper et al., 2020), peatland dynamics (Chávez et al., 2019a) as well as positive anomalies or the "greening" of "blooming deserts" in the Atacama Desert (Chávez et al., 2019b). Different from AVOCADO, all of these studies used a leave-one-out approach to determine the phenological baseline, without automatic detection of the disturbances, and without using an independent data set of an undisturbed forest to create the reference phenological curve. Any sensor or combination of sensors (e.g. Landsat and Sentinel) can be used, but in this study we test the AVOCADO algorithm using Landsat data.

The algorithm can be found in the following github page: (https://github.com/MDecuy/AVOCADO) and accompanying tutorial (http://www.pucv.cl/uuaa/labgrs/proyectos/AVOCADO).

The AVOCADO method for continuous forest disturbance and regrowth detection considers the following three steps.

Step 1: Creating the reference phenology.

The first adaptation from the original "npphen" anomaly detection method was to allow users to define the phenological baseline using a different area based on which anomaly detection is calculated. For example, undisturbed forest of the same forest type and seasonality inside a protected area can be used as a reference to study disturbances in the surrounding forest. For this reference area, a reference annual phenology is created using the "Phen" function of the "npphen" R package (Fig. 1). We used in our study sites the NDMI (Normalized Difference Moisture Index) derived from Landsat data. Fig. 1 displays the annual reference phenology of the study site of Genteguela (Ivory Coast) as an example. The reference phenology is calculated by means of a kernel density estimation of the time –space considering all the historical NDMI annual cycles of all pixels within the reference area. The yellow, orange and red colored areas represent the percentiles of the frequency of observed NDMI values across the year and the dark red line (which represents the highest frequency of observed NDMI values) is the most likely phenological annual behavior, which is set to be our reference. NDMI anomalies will be further calculated using this phenological baseline, together with the anomaly likelihood which considers the position of NDVI values in the percentiles of the NDMI frequency distribution. In the case of Genteguela (Ivory Coast), we see a strong seasonal signal for the annual phenological cycle with a peak in NDMI around DOY 250 (in September). For example, the NDMI frequency distribution in Fig. 1B around DOY 250 shows that values of NDMI below 0.1 are very unlikely (NDMI values at RFD $\geq$ 95%), and therefore,

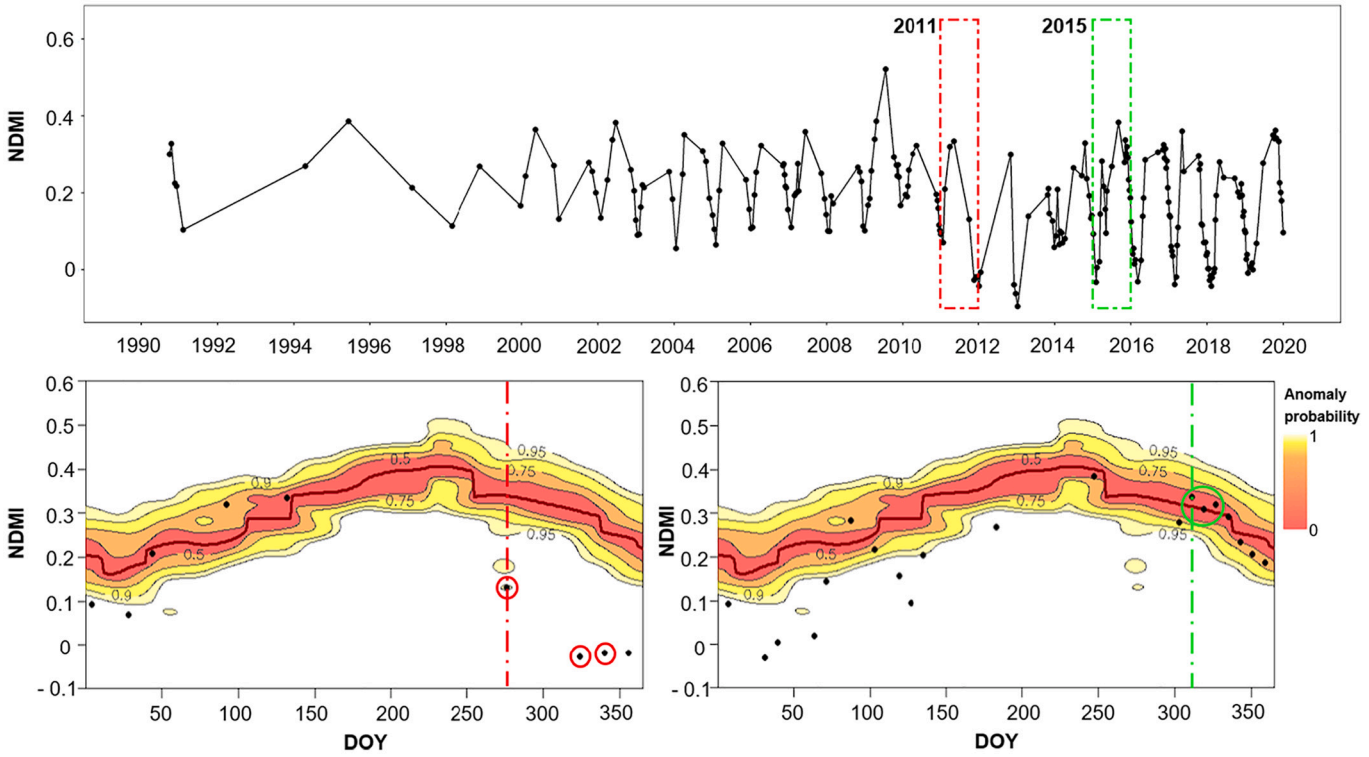

Fig. 1. The AVOCADO method for multiple disturbance and regrowth detection. A - Example of an NDMI time series for a Landsat pixel of interest (POI) in Genteguela (Ivory Coast) to be assessed. The red box delineates the data points in 2011 where the algorithm detected a disturbance with a high likelihood (outside the 95% of the reference frequency distribution or RFD $\geq$ 0.95), shown in panel B, while the green box delineates the data points in 2015 where a regrowth was detected, shown in panel C). Please note that NDMI anomaly values at RFD $\geq$ 0.95, thus the remaining 0.05 of the RFD, are extremely high or low values. B - The reference curve of (undisturbed) forest in Genteguela representing the annual phenology and its frequency distribution (yellow colors showing which NDMI values have a high likelihood of being an anomaly) for each DOY (Day of Year) with the data points for the POI of 2011. The red circles show the consecutive data points (in this study a minimum of three points) outside the 95% of the NDMI frequency distribution (RDF $\geq$ 0.95), flagging a disturbance. C - The same reference curve as in panel B, with the data points for the POI of 2015. The green circle shows the consecutive data points (in this study a minimum of three points) which are on top or above the (dark red) reference line flagging a forest regrowth. See appendix A for the reference curves for the other sites. (For interpretation of the references to colour in this figure legend, the reader is referred to the web version of this article.)

can be considered as a potential disturbance. On the other hand, if there was a disturbance at a given time, followed by forest regrowth, reaching NDMI values of about 0.3 at DOY 250 (approaching again the red line), it can be considered as potential regrowth (Fig. 1C).

Step 2: Time series anomaly and probability calculation.

After creating the reference phenology, for each pixel of interest (POI) (Fig. 1 B and C), the anomaly and its probability for each datapoint within the POI time series is calculated based on the reference. The NDMI anomalies in Fig. 1B and C are the differences between the observed NDMI (Fig. 1A) and the expected NDMI (red line in Fig. 1 B and C), and are calculated for the respective DOY. The position of the observed NDMI value within the NDMI RFD (Fig. 1 B and C - colored areas) represents the likelihood of the anomaly value, with values close to zero being frequently observed values and values $\geq$0.95 with having a very low frequency. This likelihood gives an indication of whether the anomaly is within the natural variability of the reference forest, both temporally and spatially, or indeed a "true anomaly" indicating forest disturbance. These two values per POI and date are used in further steps to evaluate and detect disturbances. For regrowth detection, only the anomalies and the reference phenology are used, not the RFD position. The R implementation of AVOCADO allows large data analyses of remote sensing time series data (raster-stacks) in parallel using multi-core computational capabilities.

Step 3: Change detection and model adaptations.

In this study we define disturbance as consecutive negative NDMI anomalies (in this study: three observations) at RFD $\geq$ 0.95. These changes can be induced by human activity or may be natural disturbances (e.g. extreme drought events or fire). We define intact forest as forest with NDMI values falling within the boundaries of natural seasonal variation (e.g. observations at RFD $<$ 0.95). Finally, regrowth is defined as the recovery of the canopy (reaching again the reference phenology) after a disturbance event. Since remote sensing data can be noisy, especially in the humid tropics due to high cloud cover, accurate disturbance and regrowth detection often cannot be achieved based on a single date. A pixel that indicates a potential change across multiple consecutive images is more likely to be land cover change. For this reason, we included several arguments in our algorithm that allow users to define thresholds to optimize detection consistency. These are:

For disturbance detection:

D-a. A candidate disturbance date is flagged when a negative NDMI value is found that is outside the reference phenology (e.g. RFD $\geq$ 95) and is called a "true anomaly" in this study (Fig. 1 B). The user can change the RFD threshold, but in this study we use RFD $\geq$ 95.

D-b. The user can also define how many consecutive data points with the above-mentioned characteristics need to be found to be considered potential disturbance. We call this parameter "cdates". For example, in Fig. 1B three consecutive dates (cdates = 3) were defined in all cases. When the condition is met, then the first of the three dates is considered as a "true anomaly". In this study we used three consecutive dates as this has been shown to give good results in other studies (Zhu et al., 2012).

D-c. When a potential date of disturbance is detected according to D-b, the user can define an additional parameter to make the detection of a real disturbance more accurate. This parameter will avoid disturbance detection in cases where regrowth is detected too soon after the flagged disturbance event, for example within a year. We call this parameter "dstrb_thr" and it can be set to any threshold period (for example dstrb_thr = 365 days), within which a candidate disturbance date is neglected if an early regrowth is detected. This potential early regrowth corresponds to three consecutive scenes with positive anomalies during 365 days from the disturbance detection date to eliminate temporally short disturbances such as drought effects. In this study we wanted to take into account all disturbances and used dstrb_thr = 0.

As the algorithm considers the whole area to be forested at a certain point in the past (before the start of the time series), therefore the AVOCADO output of the first years represent an accumulation of the disturbances before the time series and the actual changes in those initial years. If the first years of the time series have e.g. only one or two data points, detection of disturbances will be delayed, and therefore it is recommended to consider the first few years in the time series as an accumulated amount of disturbances rather than to report year-to-year disturbance rates. Alternatively, the accumulated disturbance areas can be used to create a benchmark non-forest area rather than classify one or a few satellite images to create a forest – non-forest benchmark.

For regrowth detection:

R-a. A candidate regrowth date is flagged when a zero or positive anomaly is found (Fig. 1C). A positive anomaly means that the expected value from the reference phenology has been reached again.

R-b. Identical to the disturbance detection, the users can define how many consecutive dates with the above-mentioned characteristics need to be found to flag true regrowth. Similar to the disturbance detection, the regrowth detection is also controlled by the argument "cdates". For example, in Fig. 1C and in our study three consecutive data points were defined for both disturbance and regrowth when cdates = 3.

R-c. Similar to the disturbance case, when a potential regrowth date is defined (R-b), the user can define a parameter called "rgrow_thr" to avoid regrowth detection in case a forthcoming disturbance is occurring too fast (e.g. within a year). This early new disturbance corresponds to three consecutive scenes with negative anomalies at RFD $\geq$ 0.95 during e.g. 365 days from the regrowth detection date. In this study we used 730 days since regrowth is often a long and gradual process and should thus not have a disturbance in those two following years.

2.2. Study sites

For this study three sites were selected that complement in (i) their ecological zone and thus seasonality, (ii) type of forest change, and (iii) data availability.

Madre de Dios is located in southeastern Peru (Appendix B) and part of the Amazonian rainforest, receiving about 2200 mm rainfall with a unimodal distribution throughout the year (derived from WorldClim2 - Fick and Hijmans, 2017). Deforestation is mainly driven by government subsidized agricultural expansion initiated in the 1980s and 1990s (Chavez and Perz, 2012), the construction of a major road accelerated this deforestation (Scullion et al., 2014), and more recently due to legal and illegal gold mining (Asner et al., 2013). Generally, deforestation is more abrupt (e.g. clear-cut) and over larger patches compared to the other two sites. Data availability in this site is high and relatively uniformly spread over the time series (see 2.3. Landsat, Appendix C).

The Genteguela site is located in the Woroba District in the northwest of Ivory Coast (Appendix B) and is characterized by dry sub-tropical climate. This area has a unimodal rainfall distribution (about 1240 mm) with distinct wet (rainy) and dry seasons (derived from WorldClim2 - Fick and Hijmans, 2017). The forest is classified as tropical moist deciduous forest (FAO, 2012). Deforestation in Ivory Coast is among the highest in the world, driven by agriculture, teak logging as well as cocoa and cashew encroachment, and left landscapes of fragmented forests at higher risk of further deforestation (Despretz, 2020). The deforestation is often small-scale and gradual. Data availability in this site is low, especially for the period before the year 2000 (see 2.3. Landsat, Appendix C).

The Kilosa site in Tanzania is located at the southern part of the Kilosa district around Mikumi (Appendix B) and consists of tropical dry forest and tropical shrubland ranging from lowland areas (270 m a.s.l.) predominantly used for crop production and mountainous areas (2200 m a.s.l.), including the Udzungwa Mountains National Park containing dry miombo woodland. The average annual rainfall is about 1000 mm (derived from WorldClim2 - Fick and Hijmans, 2017), with slightly less rainfall in the mountainous areas. Seasonality is strong with a dry season from June to November and a rainy season from November to May. The rainy season can be divided into short rains from November to January and long rains from March to May (Näschen et al., 2019). The

deforestation rates in Tanzania are very high. This happens in an abrupt manner (clearance of forest for crops) as well as being preceded by forest degradation (causing more gradual disturbance patterns) (Doggart et al., 2020). Major cash crops are grown in the lowlands and include cassava, rice, sorghum, maize and yams (Sills et al., 2014). Data availability in this site is low, especially before the year 2000 (see 2.3. Landsat, Appendix C).

2.3. Landsat data

All level-1 terrain-corrected (L1T) Landsat scenes were pre-processed and downloaded via the Google Earth Engine (GEE) platform (Gorelick et al., 2017). The pre-processing entailed selecting only the Landsat scenes with a cloud cover of less than 70%, clipping by the regions of interest (ROI), merging (in case of multiple paths/rows), cloud masking with the FMASK, and calculating the surface reflectance index, NDMI (Masek et al., 2006; Vermote et al., 2016). We used NDMI because of its ability to capture gradual changes and regrowth, in contrast to e.g. NDVI (DeVries et al., 2015a). The time series stacks ranged from 1990 to 2019 for the site in Peru (1063 scenes – WRS2 path/row 002/069) and the site in Ivory Coast (334 scenes - WRS2 path/row 198/054), and from 1984 to 2016 for the site in Tanzania (288 scenes - WRS2 path/rows 167/065–066). The number of scenes per year can be found in Appendix C.

2.4. Accuracy assessment

2.4.1. Sampling procedure

We assessed disturbance and regrowth accuracies for each study site in two separate assessments, following the same procedure for each. A pixel based, stratified random sampling approach was applied. For the disturbance assessment, disturbance and intact forest strata were created based on the algorithm output for each site. Since we assume the whole area to have been forest at some point in time and to account for disturbances that occurred before the observation period, we divided the disturbance stratum into "disturbance before the year 2000" (which could also be considered non-forest) and disturbance from the year 2000 onwards. In the "disturbance before the year 2000" stratum it is very difficult to separate disturbances that happened just before or at the beginning of the time series which could in some cases lead to an overestimation of the accuracy. Additionally, a buffer stratum inside the stable forest stratum was created by applying a 500 m buffer around roads or villages which can have a higher possibility of being disturbed. Because intact forest areas are generally rather large, a buffer stratum around possible disturbance areas inside the stable area can help in estimating omission errors of disturbance (Pfaff, 1999). It is referred to as "intact forest (inside buffer)" in Table 1. Because of the limited amount of very high resolution images (VHR) (which are especially needed to verify regrowth – see section "Pixel interpretation"), we selected a random sample based on the pixels with one disturbance only for the disturbance accuracy assessment. Since sample sites with multiple changes include regrowth, it would not be possible to verify the earlier regrowth due to the lack of these VHR images.

For the regrowth assessment, we created a regrowth stratum and a no-regrowth stratum based on the output of the algorithm. The no-regrowth stratum is further divided into an inside and outside buffer. No-regrowth inside buffer could indicate potential no-growth areas and can help in estimating the omission errors of regrowth. In the sites in Peru and Ivory Coast, no-growth inside areas are defined as a buffer stratum of 500 m around the (seasonal) rivers since the areas around the rivers are more dynamic and thus more likely to have forest regrowth. In the site in Tanzania, due to the similarity between dry forest and crops in NDMI signal and in some cases irrigation of crops, large areas of crops were wrongfully labelled as regrowth by the algorithm (see Discussion). Therefore we used a land cover map and masked out the crop areas (Buchhorn et al., 2020) after the initial disturbance. The regrowth stratum consisted of all pixels with exactly one disturbance and one regrowth detection. This is because high resolution satellite data are needed to verify regrowth and often only a few images are available. For that reason, sample pixels for the regrowth assessment were subset to dates close to which high-resolution imagery was available. Due to the scarcity of Landsat scenes in the 90's, we took a 5-year window for a pixel to be confirmed as disturbed in the site in Ivory Coast and Tanzania (Appendix C). For disturbance detections after 2000, a 1-year window was used. Since the site in Peru had no issues with data limitation at the start of the time series, a 1-year window was used to assess all disturbance dates. If a pixel was flagged outside this temporal window it was considered as an error.

Table 1
The sample size and mapped area proportion for each site and stratum.

Site	Stratum	Sample size	Mapped area proportion
Peru	Disturbance <2000	118	0.314
Peru	Disturbance ≥2000	105	0.229
Peru	Intact forest (inside buffer)	100	0.038
Peru	Intact forest (outside buffer)	191	0.418
Peru	Regrowth	100	0.244
Peru	No regrowth (inside buffer)	109	0.537
Peru	No regrowth (outside buffer)	100	0.220
Ivory Coast	Disturbance <2000	327	0.637
Ivory Coast	Disturbance ≥2000	287	0.330
Ivory Coast	Intact forest (inside buffer)	100	0.003
Ivory Coast	Intact forest (outside buffer)	100	0.030
Ivory Coast	Regrowth	100	0.003
Ivory Coast	No regrowth (inside buffer)	180	0.475
Ivory Coast	No regrowth (outside buffer)	198	0.522
Tanzania	Disturbance <2000	100	0.085
Tanzania	Disturbance ≥2000	100	0.058
Tanzania	Intact forest (inside buffer)	100	0.073
Tanzania	Intact forest (outside buffer)	207	0.784
Tanzania	Regrowth	100	0.198
Tanzania	No regrowth (inside buffer)	102	0.548
Tanzania	No regrowth (outside buffer)	100	0.254

Optimal sample sizes were calculated using the formula by (Cochran, 1977 - Eq. (5.25)) based on a target standard error of 0.02, for overall accuracy, and expected user's accuracies of 0.7 and 0.9 for disturbance and intact forest, and 0.6 and 0.95 for regrowth and no-regrowth, respectively. A minimum sample size of 100 per stratum was used, resulting in a total of 2924 pixels, with a minimum sample size of 800 pixels per site (Table 1). In Table 1, the mapped area proportion for each stratum can be found, summing up to one for both the disturbance and regrowth strata.

2.4.2. Pixel interpretation

The manual interpretation for the disturbance-non disturbance pixels was done by using the Landsat images. We used the TS chips R package based on the TimeSync method for change validation by Cohen et al. (2010), combined with VHR satellite images available on Google Earth (http://earth.google.com/). While disturbance pixels are relatively easy to detect, confident verification of regrowth relied on the visualization of VHR satellite images available on Google Earth.

2.4.3. Calculation of the accuracy

For each sample site, inclusion probabilities and the sample estimation weights were calculated since the sample sites have unequal inclusion probabilities across strata. Based on these, overall user's and producer's accuracies (UA and PA) (Stehman et al., 2003), and their 95% confidence intervals, as well as area estimates of each map class, were calculated following Stehman (2014). In addition, these area based metrics were supplemented by a simple sample count based confusion matrix.

3. Results

3.1. Accuracy of the AVOCADO algorithm

The AVOCADO algorithm showed very good overall accuracies for all sites, having overall accuracies of >90% for both disturbance and regrowth detections (Table 2). In general UA and PA are high (~ 90%). The site in Peru had high UA and PA, with accuracies >90% but had a slightly higher omission error in the intact forest. Also the regrowth accuracies were > 90%, with a marginally higher omission error for regrowth class (<10% of the regrowth is omitted).

Although slightly lower accuracies, the results for the site in Ivory Coast are similar, with the exception of the very low PA for the intact forest (33.8%). The low value indicates an overestimation of forest disturbance at the cost of the intact forest (see also the confusion matrix - Appendix D) The regrowth accuracies were above 90%, but the PA of the regrowth class was very low (6.1%) which indicates an overestimation of the no regrowth class. The UA and PA of the disturbance class in the site in Tanzania (respectively 82 and 79.4%) indicated an overestimation of forest disturbance. The regrowth class had a UA of 76 and a PA of 88% indicating overestimation of regrowth at the cost of an underestimation of the no regrowth class (Appendix D).

3.2. Forest disturbance and regrowth dynamics per site

3.2.1. Peru

The results show that in Madre de Dios the forest changes are often larger patches (> 1 ha) of forest cleared at once (Fig. 2A). The main disturbance activities are located along the major Inter-Oceanic Highway and rivers. The first regrowth map (Fig. 2B) shows that forest regrowth is mainly occurring in the proximity of the rivers. This is due to shifting agriculture practices in the area around the rivers, with patches of forest disturbance, cropping for two to three years generally, which is then followed by regrowth (fallow), before the forest is cleared again for cropping. A large part of the changes in the last decade are related to mining. Fig. 3 shows an example of one pixel that had multiple changes due to shifting cultivation. The forest was cleared in 2000, while in 2004 we see a forest recovery (cauliflower like tree canopies) on the VHR image, while in 2008 it was cleared again for cultivating crops in 2011. In 2013 it seems no crops are cultivated anymore and in 2015 early signs of forest recovery can be seen. At the end of 2016 the pixel was labelled by the algorithm as regrown, which is confirmed by the images in 2016 and 2018.

The average annual disturbance rate (2000–2019), derived from the forest change output, was about 0.47%, with the highest disturbance rate recorded in 2005. The regrowth rates were relatively high, with an average of 0.84% (2000–2019). Fig. 4A shows the derived proportions of intact forest, secondary forest and non-forest areas per year. In 2019, about 46% of the area is covered with intact forest, while 17% of the area consists of secondary forest, and 37% is non-forest.

3.2.2. Ivory coast

Most of the site in Ivory Coast was disturbed in the 1990s or before, especially in the western part of the site (Fig. 2C). Most of the recent disturbance that could be verified with high spatial resolution images (Google Earth) is due to small scale selective logging. Regrowth is often small scale and spatially scattered, due to the recovery or expansion of the canopies of surrounding trees. The larger areas of regrowth might not be natural forest regrowth, but rather plantations of cacao (*Theobroma cacao*) or cashew (*Anacardium occidentale*) trees. These are grown below or alongside natural forest as they require shade. An example of a (verified) location with cacao plantation is shown in Appendix F. The time series indicates more subtle disturbance patterns compared to conversion to oil palm plantations (Appendix F) as for cacao only a selective number of trees are harvested, and the forest gaps are slowly filled by the maturing cacao trees. The disturbance rates are very high,

Table 2
Area weighted accuracies (OA = overall accuracy; UA = user accuracy or commission errors; PA = producer accuracy or omission errors) and their 95% confidence interval (CI) for all sites and the area weighted estimates (ha) and standard error (SE).

Disturbance strata	OA (±CI)	UA (±CI)	PA (±CI)	Sample based area estimate (ha) (SE)	Map area (ha)	Δ Sample based area estimate and map area (ha)
Peru	95.1 (2.3)					
Disturbance <2000		93.2 (4.6)	99.4 (1.1)	60,626 (1540)	48,575	12,051
Disturbance ≥2000		92.4 (5.1)	98.5 (2.8)	33,211 (1042)	35,424	−2213
Intact forest		99.1 (1.7)	88.9 (5.0)	60,755 (1802)	70,592	−9837
Ivory Coast	93.2 (2.0)					
Disturbance <2000		92.7 (2.8)	99.4 (0.7)	6018 (95)	6453	−435
Disturbance ≥2000		93.7 (2.8)	99.8 (0.3)	3136 (48)	3339	−203
Intact forest		97.2 (3.0)	33.8 (7.0)	979 (103)	341	638
Tanzania	94.0 (2.2)					
Disturbance <2000		82.0 (7.6)	79.4 (18.1)	22,710 (2154)	21,978	732
Disturbance ≥2000		77.0 (8.3)	73.9 (13.6)	15,769 (2063)	15,126	643
Intact forest		96.4 (2.4)	97.0 (0.9)	221,097 (2927)	222,473	−1376
Regrowth strata	**OA (±CI)**	**UA (±CI)**	**PA (±CI)**	**Sample based area estimate (ha) (SE)**	**Map area (ha)**	**Δ Sample based area estimate and map area (ha)**
Peru	98.1 (1.8)					
No regrowth		98.1 (2.1)	99.4 (0.8)	39,287 (459)	48,575	12,051
Regrowth		98.0 (2.8)	93.6 (6.7)	11,730 (459)	12,425	−2213
Ivory Coast	96.0 (2.0)					
No regrowth		92.7 (2.8)	99.4 (0.7)	6018 (95)	6453	−435
Regrowth		93.7 (2.8)	99.8 (0.3)	3136 (48)	3339	−203
Tanzania	91.2 (3.1)					
No regrowth		82.0 (7.6)	79.4 (18.1)	22,710 (2154)	21,978	732
Regrowth		77.0 (8.3)	73.9 (13.6)	15,769 (2063)	15,126	643

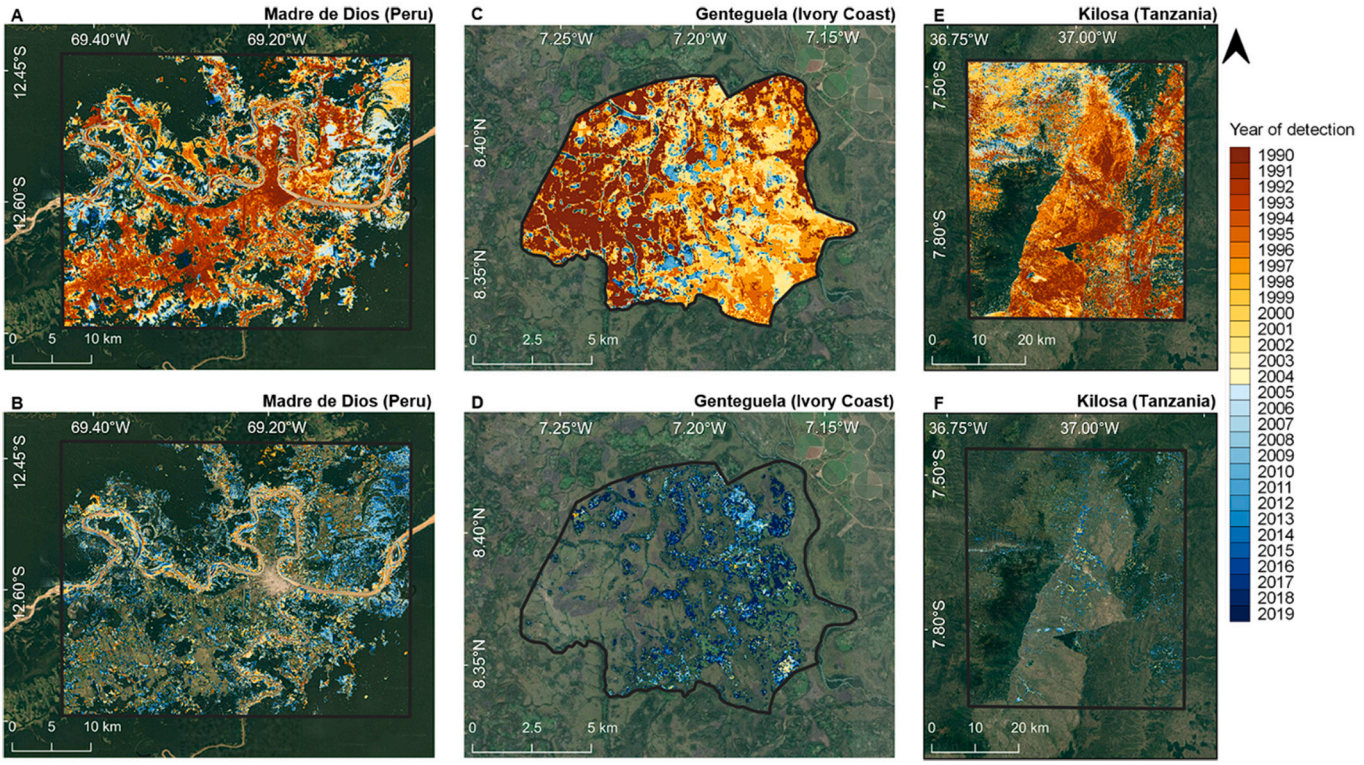

Fig. 2. Top row (panels A, C, E) shows the first year of the disturbance detection for each site (see legend on the right). The bottom row (panels B, D, F) shows the first year of regrowth for each site. The 2nd to 4th disturbance and regrowth cycles can be found in appendix E. The annual forest disturbance and regrowth maps can be interactively viewed by clicking on the following link: https://dashboards.icraf.org/app/avocado_fcm.

and by the end of 2019 most of the intact forest had disappeared (only 2.5% remained – Fig. 4B). The average annual disturbance rate (2000–2019) was about 1.46%, while the regrowth rate (0.20%) was low compared to the site in Peru. The majority of the intact forest can be found along the seasonal streams running through the area. The proportion of secondary forest at the end of 2019 was 4%, and the non-forest area was about 94% (Fig. 4B).

3.2.3. Tanzania

The site in Tanzania is characterized by a large area in the centre that was deforested for intensive crop production. Most of that area was already cleared before the start of our time series analysis in 1984 (Fig. 2E). Other disturbances can be found in the east and in the north-west corner, while in the national park in the south-west almost no changes occurred. Most of the recent changes (last decade) that could be verified with high spatial resolution images (Google Earth) are small scale degradation, mostly along the forest edge. In Appendix F we can see an example of small-scale encroachment along the forest edge, captured by the AVOCADO algorithm. The average annual disturbance rate (2000–2015) was about 0.59%, similar to the site in Peru, and the regrowth rate was 0.27%, similar to the site in Ivory Coast. Since the area consists of a protected national park, the proportion of intact forest is relatively high compared to the other sites (about 58.85% by the end of 2015). Similar to the site in Ivory Coast, the proportion of secondary forest is low with 4.60%, and the non-forest area is about 36.54% by the end of 2015 (Fig. 4C).

4. Discussion

4.1. Robustness of the algorithm to deal with seasonality and climate extremes

In this study we introduced the AVOCADO algorithm and its performance with three complementary sites with differences in seasonality, data availability, and type of disturbance. Overall the accuracies were good, with some variation between the sites.

The high accuracies in the site in Peru (OA, PA and UA > 90%) are most likely due to the low seasonal variability and the high data density in that site. The peak in disturbance in 2005 is partially caused by an extreme drought (El Niño event) in that year (Frappart et al., 2012; Marengo et al., 2008). Although a true disturbance, this might be considered as noise when it comes to deforestation monitoring (e.g. REDD+ monitoring). In such cases that year could be excluded in the postprocessing process with the risk of eliminating actual deforestation events, or by setting the "dstrb_thr" parameter of the AVOCADO algorithm to e.g. one year. However, when applying this parameter, care has to be taken to avoid omission errors in areas with rapid forest regrowth which is the case in this site.

The site in Ivory Coast has a stronger seasonality and is more heterogeneous in terms of land cover than the site in Peru, which affected the producer accuracy (PA) of the disturbance detection in the Ivory Coast site. The low producer accuracy of respectively 33.8% and 6.1% in the stable forest and regrowth class indicates that the algorithm overestimated disturbance and non-forest. Since these classes are small, relative to the disturbance classes (Table 2), the errors of the omission estimation can be aggravated, leading to low PA's (Olofsson et al., 2020). The accuracy estimation of these classes could be improved by a better stratification of the large disturbance classes (Olofsson et al., 2020). In the Ivory Coast site, most commission errors in the disturbance detection were due to small patches with a different forest type growing along seasonal streams and rivers. Although it considers a very small proportion of the area, separating the two forest types and using separate reference phenologies could improve the results.

The site in Tanzania had lower disturbance and regrowth accuracies compared to the other two sites due to its strong seasonality (Hamunyela et al., 2020). Since we used dry miombo forest for the forest reference

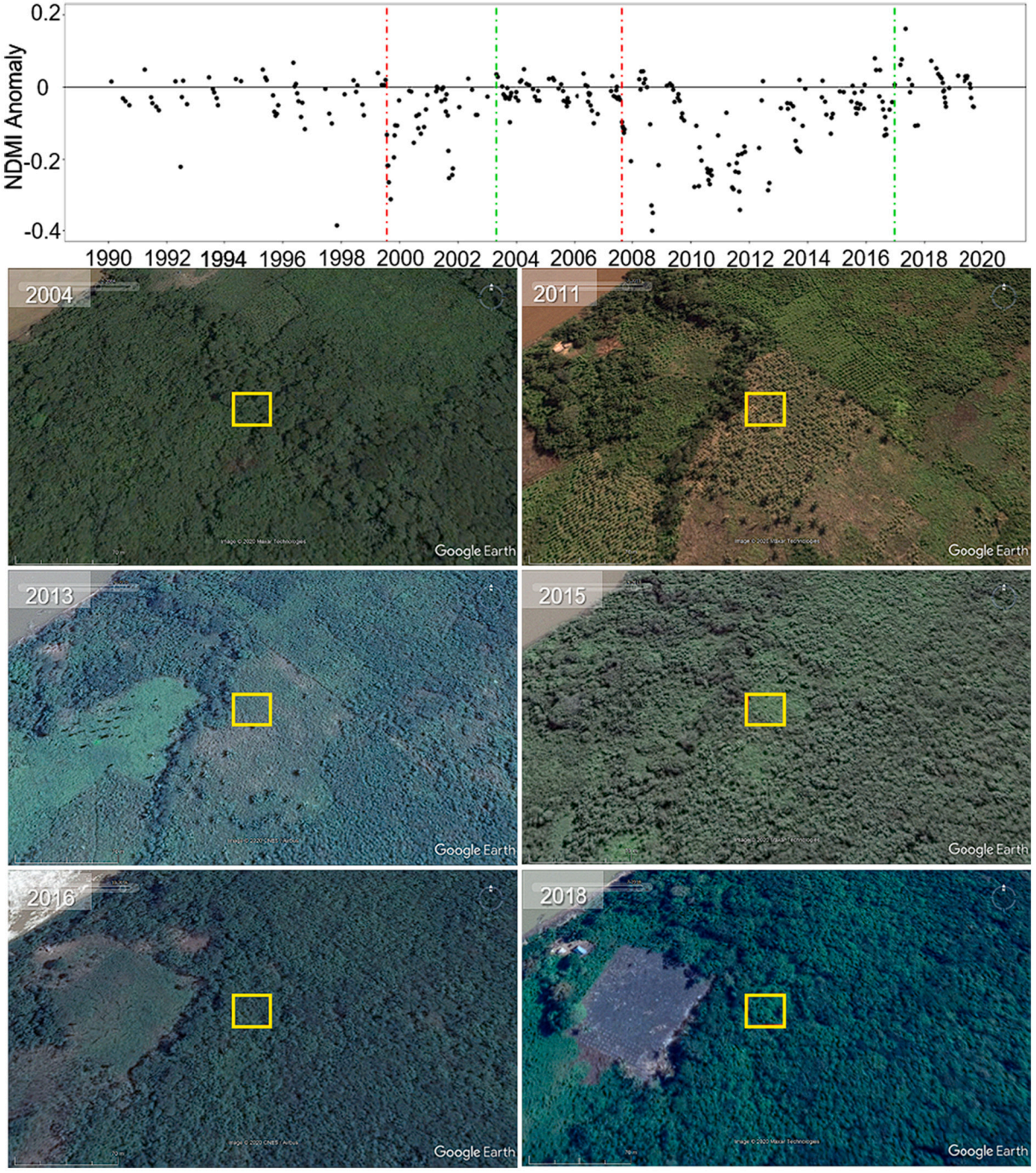

Fig. 3. Example of shifting agriculture in Madre de Dios (Peru) - (12°40′16" S; 69°13′14" W). Top: Pixel time series of the NDMI anomalies with disturbances indicated by red vertical lines and regrowth by green vertical lines. Below: Images from Google Earth with the pixel of interest (yellow rectangle). (For interpretation of the references to colour in this figure legend, the reader is referred to the web version of this article.)

curve, the disturbance accuracies are still relatively high considering the challenges with the strong seasonal influence on the forest phenology. Most of the disturbance commission errors were due to a late detection of the change as a consequence of the lower data availability and wrong detections as a consequence of years with a very strong or early dry season. This was also the case for other change detection methods, which showed low PA's for a site similar to the one used in this study in Tanzania (Bos et al., 2019). The dry and often scarce forest cover is probably the reason of the relatively low accuracies for the regrowth detection compared to the other sites. As all the commission errors in the regrowth detection were in areas where the follow-up land use was pasture and crops, it seems that the NDMI reflectance of that type of vegetation, especially when irrigated, looks similar to the NDMI reflectance of forest (especially miombo forest). Here, the use of other vegetation indices should be explored. For example, NDVI should perform well in arid and semi-arid ecosystems since the NDVI reflectance is unlikely to saturate in these ecosystems (Cui et al., 2013). Another option is to use post-disturbance classifications where regrowth is classified in e.g. natural regrowth, plantations and other land-use types (Hermosilla et al., 2018). Since the reference phenology has been based on ~30 years of data, the algorithm is potentially more robust in sites with strong seasonal variety then other change detection

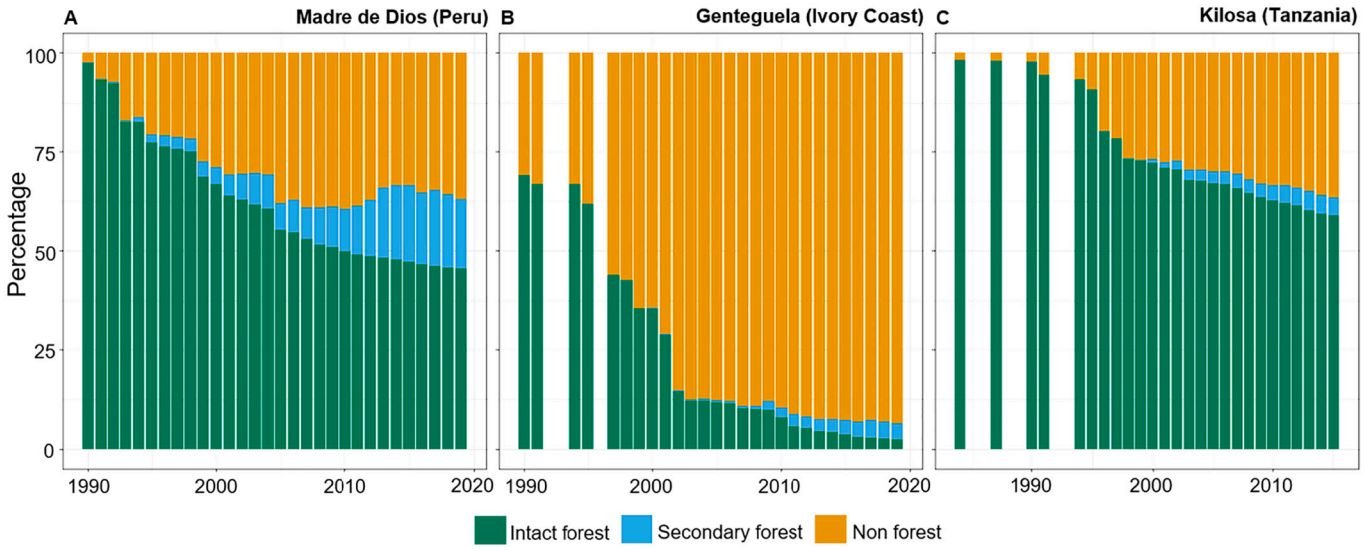

Fig. 4. The percentage of intact forest, secondary forest, and non-forest for the three sites: A - Madre de Dios (Peru), B - Genteguela (Ivory Coast), C - Kilosa (Tanzania). (For interpretation of the references to colour in this figure legend, the reader is referred to the web version of this article.)

methods as it takes small shifts in year-to-year seasonality into account.

4.2. Robustness of the algorithm to deal with different types of changes

In the site in Peru, a common practice of (smallholder) farmers is to convert primary forests into shifting cultivation mosaics, leaving the forest to recover after a few years of crop cultivation, and before cutting the forest again for another rotation cycle (Ravikumar et al., 2017). The change detection results (Fig. 4) confirm this by the relatively large proportion of secondary forest, and the specific examples (Fig. 3 and Appendix F) indicate that the algorithm is capable of detecting the relatively fast changing forest, non-forest dynamics. The figure in Appendix F also shows one of the other major drivers of deforestation in the Madre de Dios region, which is illegal gold mining (Asner et al., 2013; Scullion et al., 2014).

In many sub-Saharan African countries, deforestation is driven by smallholder subsistence agriculture (Fisher, 2010), with forest changes at small spatial scale and often very gradual over time (DeVries et al., 2015b). This is also the case for the sites in Ivory Coast and Tanzania, but in both areas large parts were already deforested before the start of our time series analysis and a large area was an accumulation of past disturbances (basically non-forest) in the first years of our monitoring period. Similar to previous studies, we found that a large area was disturbed in Ivory Coast, with selective logging for Cacao plantations being an important driver (Despretz, 2020; Wessel and Quist-Wessel, 2015). More recent changes show single pixel or small clusters of pixels indicating disturbance (Fig. 2, Appendix E). These probably result from selective logging for cacao plantations and forest edge degradation (see time series examples in Appendix F) which are quite commonly found in the areas. Our algorithm is able to detect such changes which is important to accurately account for deforestation and derived carbon stock change estimations in smallholder agricultural dominated landscapes (Tyukavina et al., 2013).

4.3. General strengths and limitations to the method

Our study shows that the probabilistic based AVOCADO algorithm creates a robust forest reference, taking all data, and thus the natural variability between years into account. For the algorithm to perform accurately, it is crucial that the user selects the reference forest area carefully. The forest reference is not necessarily taken inside the area of interest, which has the advantage that it does not require a part of the time series to be used as training data, and it speeds up the processing time. But the reference forest should be representative for the forest in the area of interest (i.e. forest within the area of interested should have very similar phenological curves) and be undisturbed. Also, the algorithm does not require a benchmark non-forest mask. The downside is that this poses limitations in applying the algorithm to large areas. High accuracies are conditional on homogenous phenological patterns. When applying to larger spatial scales, a benchmark classification of phenologically different forest types is required and the method needs to be applied separately to the different forest classes that have different phenological patterns, making the AVOCADO algorithm increasingly laborious with increasing spatial scales that are likely to include a variety of forest types. In principle the algorithm can be used with a variety of data coming from different sensors (e.g. Sentinel combined with Landsat), but the robustness of the reference phenology will decline with shorter time series.

The algorithm has potential to be used for monitoring other vegetation changes associated to land cover transitions, such as grassland to cropland transitions, but more research to assess the algorithm's performance across different contexts is needed.

4.4. Application for forest monitoring for conservation and restoration

Forest disturbance is not always abrupt, it is often preceded by selective logging and degradation (Vancutsem et al., 2020). Such gradual disturbances have a large impact on conservation and threaten the success of efforts to reduce emissions such as REDD+ (Reducing Emissions from Deforestation and forest Degradation) (Angelsen et al., 2018; Matricardi et al., 2020). To date it has been difficult to monitor gradual changes using time series analyses with remote sensing methods (Mitchell et al., 2017). The current algorithm demonstrates an ability to detect forest degradation which is an important advance to monitoring effectiveness of conservation efforts.

Forest regrowth is key to achieving restoration targets (e.g. Chazdon and Guariguata, 2016). However, due to its gradual nature forest regrowth is harder to detect than deforestation, and to date regrowth is rarely assessed in a continuous way in remote sensing studies. This is particularly relevant in systems with strong human-induced changes in land cover, including agroforestry and shifting cultivation systems, which require continuous forest change detection. One study assessing regrowth reported that only 27% of the forest loss is a permanent land use change (Curtis et al., 2018). The results of the algorithm provide

information on where forest is recovering, and how long a secondary forest is able to persist. The resulting forest regrowth maps are important to assess the potential of regrowth forests for restoration (e.g. Cook-Patton et al., 2020).

5. Conclusion

Here we present a new algorithm, coined AVOCADO, that enables the assessment of forest disturbance and regrowth in a continuous and robust way. We demonstrate its accuracy in sites that are complementary in climate and disturbance regimes. Main improvements compared to previously published algorithms are that: a) AVOCADO is sensitive to gradual changes and thereby able to accurately detect forest degradation and forest regrowth; b) it allows for multiple disturbance and regrowth detection; c) it allows forest monitoring from the beginning of the satellite time series; d) it provides several arguments to help users fine-tune detection results (RDF value accounting for anomaly detection likelihood, 'cdates' accounting for consecutive dates to ensure detection, 'dstrb_thr' and 'rgrow_thr' accounting for minimum period before we can expect disturbance or regrowth). A critical step of the AVOCADO approach is the definition of a valid reference area, from which the phenological baseline is defined. Finding a representative reference area for large areas can be a limitation on the use of this method. The above mentioned improvements are of great importance for monitoring forest conservation (e.g. under REDD) and for supporting forest restoration efforts (e.g. under the Bonn Challenge). The algorithm is open access and user friendly to a wide range of end-users.

Declaration of Competing Interest

None

Acknowledgements

M.D. acknowledges the support of the "Cocoa Land Survey (CCLS) project (V4C – MARS 101369). RCh thanks FONDECYT Iniciación N°11171046, FONDECYT Regular N°1211924. ML was supported by research programme ALW-VENI (863.15.017), financed by the Netherlands Organisation for Scientific Research (NWO) and by the CGIAR Program on Forests, Trees and Agroforestry (FTA).

Appendix A. Supplementary data

Supplementary data to this article can be found online at https://doi.org/10.1016/j.rse.2021.112829.

References

Anees, A., Aryal, J., 2014. Near-real time detection of beetle infestation in pine forests using MODIS data. IEEE J. Sel. Top. Appl. Earth Obs. Remote Sens. 7, 3713–3723. https://doi.org/10.1109/JSTARS.2014.2330830.

Anees, A., Olivier, J.C., O'Rielly, M., Aryal, J., 2013. Detecting beetle infestations in pine forests using MODIS NDVI time-series data. In: 2013 IEEE International Geoscience and Remote Sensing Symposium - IGARSS, pp. 3329–3332. https://doi.org/10.1109/IGARSS.2013.6723540.

Angelsen, A., Martius, C., De Sy, V., Duchelle, A.E., Larson, A.M., Pham, T.T., 2018. REDD+ enters its second decade. In: Angelsen, A., Martius, C., De Sy, V., Duchelle, A. E., L.A. and P.T (Eds.), Transforming REDD+: Lessons and New Directions. CIFOR, Bogor, Indonesia, pp. 1–13.

Asner, G.P., Llactayo, W., Tupayachi, R., Luna, E.R., 2013. Elevated rates of gold mining in the Amazon revealed through high-resolution monitoring. Proc. Natl. Acad. Sci. U. S. A. 110, 18454–18459. https://doi.org/10.1073/pnas.1318271110.

Bos, A.B., De Sy, V., Duchelle, A.E., Herold, M., Martius, C., Tsendbazar, N.-E., 2019. Global data and tools for local forest cover loss and REDD+ performance assessment: accuracy, uncertainty, complementarity and impact. Int. J. Appl. Earth Obs. Geoinf. 80, 295–311. https://doi.org/10.1016/j.jag.2019.04.004.

Bowman, D.M.J.S., Moreira-Muñoz, A., Kolden, C.A., Chávez, R.O., Muñoz, A.A., Salinas, F., González-Reyes, Á., Rocco, R., de la Barrera, F., Williamson, G.J., Borchers, N., Cifuentes, L.A., Abatzoglou, J.T., Johnston, F.H., 2019. Human–environmental drivers and impacts of the globally extreme 2017 Chilean fires. Ambio 48, 350–362. https://doi.org/10.1007/s13280-018-1084-1.

Broich, M., Huete, A., Paget, M., Ma, X., Tulbure, M., Coupe, N.R., Evans, B., Beringer, J., Devadas, R., Davies, K., Held, A., 2015. A spatially explicit land surface phenology data product for science, monitoring and natural resources management applications. Environ. Model. Softw. 64, 191–204. https://doi.org/10.1016/j.envsoft.2014.11.017.

Buchhorn, M., Smets, B., Bertels, L., De Roo, B., Lesiv, M., Tsendbazar, N.E., Herold, M., Fritz, S., 2020. Copernicus Global Land Service: Land Cover 100m: Collection 3: Epoch 2015: Globe [WWW Document]. https://doi.org/10.5281/zenodo.3939038.

Chavez, A.B., Perz, S.G., 2012. Adoption of policy incentives and land use: lessons from frontier agriculture in southeastern Peru. Hum. Ecol. 40, 525–539. https://doi.org/10.1007/s10745-012-9494-3.

Chávez, R.O., Estay, S.A., Riquelme, G., 2017. Npphen. Vegetation Phenological Cycle and Anomaly Detection Using Remote Sensing Data.

Chávez, R.O., Christie, D.A., Olea, M., Anderson, T.G., 2019a. A multiscale productivity assessment of high Andean Peatlands across the Chilean Altiplano using 31 years of Landsat imagery. Remote Sens. https://doi.org/10.3390/rs11242955.

Chávez, R.O., Moreira-Muñoz, A., Galleguillos, M., Olea, M., Aguayo, J., Latín, A., Aguilera-Betti, I., Muñoz, A.A., Manríquez, H., 2019b. GIMMS NDVI time series reveal the extent, duration, and intensity of "blooming desert" events in the hyper-arid Atacama Desert, Northern Chile. Int. J. Appl. Earth Obs. Geoinf. 76, 193–203. https://doi.org/10.1016/j.jag.2018.11.013.

Chávez, R.O., Rocco, R., Gutiérrez, A., Dörner, M., Estay, S., 2019c. A self-calibrated non-parametric time series analysis approach for assessing insect defoliation of broad-leaved deciduous Nothofagus pumilio forests. Remote Sens. 11, 204. https://doi.org/10.3390/rs11020204.

Chazdon, R.L., Guariguata, M.R., 2016. Natural regeneration as a tool for large-scale forest restoration in the tropics: prospects and challenges. Biotropica 48, 716–730. https://doi.org/10.1111/btp.12381.

Chazdon, R.L., Uriarte, M., 2016. Natural regeneration in the context of large-scale forest and landscape restoration in the tropics. Biotropica 48, 709–715. https://doi.org/10.1111/btp.12409.

Chazdon, R.L., Broadbent, E.N., Rozendaal, D.M.A., Bongers, F., Zambrano, A.M.A., Aide, T.M., Balvanera, P., Becknell, J.M., Boukili, V., Brancalion, P.H.S., Craven, D., Almeida-Cortez, J.S., Cabral, G.A.L., de Jong, B., Denslow, J.S., Dent, D.H., DeWalt, S.J., Dupuy, J.M., Durán, S.M., Espírito-Santo, M.M., Fandino, M.C., César, R.G., Hall, J.S., Hernández-Stefanoni, J.L., Jakovac, C.C., Junqueira, A.B., Kennard, D., Letcher, S.G., Lohbeck, M., Martínez-Ramos, M., Massoca, P., Meave, J. A., Mesquita, R., Mora, F., Muñoz, R., Muscarella, R., Nunes, Y.R.F., Ochoa-Gaona, S., Orihuela-Belmonte, E., Peña-Claros, M., Pérez-García, E.A., Piotto, D., Powers, J.S., Rodríguez-Velazquez, J., Romero-Pérez, I.E., Ruíz, J., Saldarriaga, J.G., Sanchez-Azofeifa, A., Schwartz, N.B., Steininger, M.K., Swenson, N.G., Uriarte, M., van Breugel, M., van der Wal, H., Veloso, M.D.M., Vester, H., Vieira, I.C.G., Bentos, T.V., Williamson, G.B., Poorter, L., 2016. Carbon sequestration potential of second-growth forest regeneration in the Latin American tropics. Sci. Adv. 2, e1501639 https://doi.org/10.1126/sciadv.1501639.

Cochran, W.G., 1977. Sampling Techniques, 3rd ed. John Wiley & Sons, New York.

Cohen, W.B., Yang, Z., Kennedy, R., 2010. Detecting trends in forest disturbance and recovery using yearly Landsat time series: 2. TimeSync — Tools for calibration and validation. Remote. Sens. Environ. 114 (12), 2911–2924. https://doi.org/10.1016/j.rse.2010.07.010.

Cook-Patton, S.C., Leavitt, S.M., Gibbs, D., Harris, N.L., Lister, K., Anderson-Teixeira, K.J., Briggs, R.D., Chazdon, R.L., Crowther, T.W., Ellis, P.W., Griscom, H.P., Herrmann, V., Holl, K.D., Houghton, R.A., Larrosa, C., Lomax, G., Lucas, R., Madsen, P., Malhi, Y., Paquette, A., Parker, J.D., Paul, K., Routh, D., Roxburgh, S., Saatchi, S., van den Hoogen, J., Walker, W.S., Wheeler, C.E., Wood, S.A., Xu, L., Griscom, B.W., 2020. Mapping carbon accumulation potential from global natural forest regrowth. Nature 585, 545–550. https://doi.org/10.1038/s41586-020-2686-x.

Coppin, P., Jonckheere, I., Nackaerts, K., Muys, B., Lambin, E., 2004. Review ArticleDigital change detection methods in ecosystem monitoring: a review. Int. J. Remote Sens. 25, 1565–1596. https://doi.org/10.1080/0143116031000101675.

Crouzeilles, R., Ferreira, M.S., Chazdon, R.L., Lindenmayer, D.B., Sansevero, J.B.B., Monteiro, L., Iribarrem, A., Latawiec, A.E., Strassburg, B.B.N., 2017. Ecological restoration success is higher for natural regeneration than for active restoration in tropical forests. Sci. Adv. 3, e1701345 https://doi.org/10.1126/sciadv.1701345.

Cui, X., Gibbes, C., Southworth, J., Waylen, P., 2013. Using remote sensing to quantify vegetation change and ecological resilience in a semi-arid system. Land 2, 108–130. https://doi.org/10.3390/land2020108.

Curtis, P.G., Slay, C.M., Harris, N.L., Tyukavina, A., Hansen, M.C., 2018. Classifying drivers of global forest loss. Science (80-.) 361. https://doi.org/10.1126/science.aau3445, 1108 LP – 1111.

de Beurs, K.M., Henebry, G.M., 2010. Spatio-temporal statistical methods for modelling land surface phenology. In: Hudson, I., Keatley, M. (Eds.), Phenological Research. Springer, Netherlands, Dordrecht, pp. 177–208. https://doi.org/10.1007/978-90-481-3335-2_9.

Decuyper, M., Chávez, R.O., Čufar, K., Estay, S.A., Clevers, J.G.P.W., Prislan, P., Gričar, J., Črepinšekg, Z., Merela, M., de Luis, M., Serrano Notivoli, R., Martinez del Castillo, E., Rozendaal, D.M.A., Bongers, F., Herold, M., Sass-Klaassen, U., 2020. Spatio-temporal assessment of beech growth in relation to climate extremes in Slovenia – an integrated approach using remote sensing and tree-ring data. Agric. For. Meteorol. 287, NA. https://doi.org/10.1016/j.agrformet.2020.107925.

Despretz, P., 2020. State and Trends of Deforestation in Côte d'Ivoire (2019–2020). London, UK.

DeVries, B., Decuyper, M., Verbesselt, J., Zeileis, A., Herold, M., Joseph, S., 2015a. Tracking disturbance-regrowth dynamics in tropical forests using structural change detection and Landsat time series. Remote Sens. Environ. 169 https://doi.org/10.1016/j.rse.2015.08.020.

DeVries, B., Verbesselt, J., Kooistra, L., Herold, M., 2015b. Robust monitoring of small-scale forest disturbances in a tropical montane forest using Landsat time series. Remote Sens. Environ. 161, 107–121. https://doi.org/10.1016/j.rse.2015.02.012.
Doggart, N., Morgan-Brown, T., Lyimo, E., Mbilinyi, B., Meshack, C.K., Sallu, S.M., Spracklen, D.V., 2020. Agriculture is the main driver of deforestation in Tanzania. Environ. Res. Lett. 15, 34028. https://doi.org/10.1088/1748-9326/ab6b35.
Dutrieux, L.P., Jakovac, C.C., Latifah, S.H., Kooistra, L., 2016. Reconstructing land use history from Landsat time-series: case study of a swidden agriculture system in Brazil. Int. J. Appl. Earth Obs. Geoinf. 47, 112–124. https://doi.org/10.1016/j.jag.2015.11.018.
Estay, S.A., Chávez, R.O., 2018. npphen: an R-package for non-parametric reconstruction of vegetation phenology and anomaly detection using remote sensing. bioRxiv 301143. https://doi.org/10.1101/301143.
Estay, S.A., Chávez, R.O., Rocco, R., Gutiérrez, A.G., 2019. Quantifying massive outbreaks of the defoliator moth Ormiscodes amphimone in deciduous Nothofagus-dominated southern forests using remote sensing time series analysis. J. Appl. Entomol. 143, 787–796. https://doi.org/10.1111/jen.12643.
FAO, 2010. Global Forest Resources Assessment 2010. Chapter 2: Extent of Forest Resources. Rome.
FAO, 2012. Global Ecological Zones for FAO Forest Reporting: 2010 Update. Forest Resources Assessment Working Paper 179. Rome.
Fick, S.E., Hijmans, R.J., 2017. WorldClim 2: new 1-km spatial resolution climate surfaces for global land areas. Int. J. Climatol. 37, 4302–4315. https://doi.org/10.1002/joc.5086.
Fisher, B., 2010. African exception to drivers of deforestation. Nat. Geosci. 3, 375–376. https://doi.org/10.1038/ngeo873.
Frappart, F., Papa, F., Santos da Silva, J., Ramillien, G., Prigent, C., Seyler, F., Calmant, S., 2012. Surface freshwater storage and dynamics in the Amazon basin during the 2005 exceptional drought. Environ. Res. Lett. 7, 44010. https://doi.org/10.1088/1748-9326/7/4/044010.
Gorelick, N., Hancher, M., Dixon, M., Ilyushchenko, S., Thau, D., Moore, R., 2017. Google Earth Engine: planetary-scale geospatial analysis for everyone. Remote Sens. Environ. 202, 18–27. https://doi.org/10.1016/j.rse.2017.06.031.
Griffiths, P., Kuemmerle, T., Baumann, M., Radeloff, V.C., Abrudan, I.V., Lieskovsky, J., Munteanu, C., Ostapowicz, K., Hostert, P., 2014. Forest disturbances, forest recovery, and changes in forest types across the Carpathian ecoregion from 1985 to 2010 based on Landsat image composites. Remote Sens. Environ. 151, 72–88. https://doi.org/10.1016/j.rse.2013.04.022.
Gutiérrez, Á.G., Chávez, R.O., Domínguez-Concha, J.A., Gibson-Carpintero, S., Guerrero, I.P., Rocco, R., Urra, V.D., Estay, S.A., 2020. In: Estay, S.A. (Ed.), Ormiscodes Amphimone Outbreak Frequency Increased Since 2000 in Subantarctic Nothofagus Pumilio Forests of Chilean Patagonia BT - Forest Pest and Disease Management in Latin America: Modern Perspectives in Natural Forests and Exotic Plantations. Springer International Publishing, Cham, pp. 61–75. https://doi.org/10.1007/978-3-030-35143-4_5.
Hamunyela, E., Brandt, P., Shirima, D., Do, H.T.T., Herold, M., Roman-Cuesta, R.M., 2020. Space-time detection of deforestation, forest degradation and regeneration in montane forests of Eastern Tanzania. Int. J. Appl. Earth Obs. Geoinf. 88, 102063 https://doi.org/10.1016/j.jag.2020.102063.
Hansen, M.C., Potapov, P.V., Moore, R., Hancher, M., Turubanova, S.A., Tyukavina, A., Thau, D., Stehman, S.V., Goetz, S.J., Loveland, T.R., Kommareddy, A., Egorov, A., Chini, L., Justice, C.O., Townshend, J.R.G., 2013. High-resolution global maps of 21st-century forest cover change. Science 342, 850–853. https://doi.org/10.1126/science.1244693.
Hermosilla, T., Wulder, M.A., White, J.C., Coops, N.C., Hobart, G.W., 2018. Disturbance-informed annual land cover classification maps of Canada's forested ecosystems for a 29-year Landsat time series. Can. J. Remote. Sens. 44, 67–87. https://doi.org/10.1080/07038992.2018.1437719.
Huang, C., Goward, S.N., Masek, J.G., Thomas, N., Zhu, Z., Vogelmann, J.E., 2010. An automated approach for reconstructing recent forest disturbance history using dense Landsat time series stacks. Remote Sens. Environ. 114, 183–198. https://doi.org/10.1016/j.rse.2009.08.017.
Jakovac, C.C., Dutrieux, L.P., Siti, L., Peña-Claros, M., Bongers, F., 2017. Spatial and temporal dynamics of shifting cultivation in the middle-Amazonas river: expansion and intensification. PLoS One 12, e0181092.
Kennedy, R.E., Yang, Z., Cohen, W.B., 2010. Detecting trends in forest disturbance and recovery using yearly Landsat time series: 1. LandTrendr — temporal segmentation algorithms. Remote Sens. Environ. 114, 2897–2910. https://doi.org/10.1016/j.rse.2010.07.008.
Kennedy, R.E., Yang, Z., Cohen, W.B., Pfaff, E., Braaten, J., Nelson, P., 2012. Spatial and temporal patterns of forest disturbance and regrowth within the area of the Northwest Forest Plan. Remote. Sens. Environ. 122, 117–133. https://doi.org/10.1016/j.rse.2011.09.024.
Kennedy, R.E., Andréfouët, S., Cohen, W.B., Gómez, C., Griffiths, P., Hais, M., Healey, S. P., Helmer, E.H., Hostert, P., Lyons, M.B., Meigs, G.W., Pflugmacher, D., Phinn, S.R., Powell, S.L., Scarth, P., Sen, S., Schroeder, T.A., Schneider, A., Sonnenschein, R., Vogelmann, J.E., Wulder, M.A., Zhu, Z., 2014. Bringing an ecological view of change to Landsat-based remote sensing. Front. Ecol. Environ. 12, 339–346. https://doi.org/10.1890/130066.
Lohbeck, M., Poorter, L., Paz, H., Pla, L., van Breugel, M., Martínez-Ramos, M., Bongers, F., 2012. Functional diversity changes during tropical forest succession. Perspect. Plant Ecol. Evol. Syst. 14, 89–96. https://doi.org/10.1016/j.ppees.2011.10.002.
Lohbeck, M., Poorter, L., Martinez-Ramos, M., Bongers, F., 2015. Biomass is the main driver of changes in ecosystem process rates during tropical forest succession. Ecology 96, 1242–1252. https://doi.org/10.1890/14-0472.1.
Lohbeck, M., DeVries, B., Bongers, F., Martinez-Ramos, M., Navarrete-Segueda, A., Nicasio-Arzeta, S., Siebe, C., Pingarroni, A., Wies, G., Decuyper, M., 2021. Mexican agricultural frontier communities differ in forest dynamics with consequences for conservation and restoration (in review). Environ. Res. Lett. https://doi.org/10.32942/osf.io/qxje8.
Mananze, S., Pôças, I., Cunha, M., 2020. Mapping and assessing the dynamics of shifting agricultural landscapes using Google earth engine cloud computing, a case study in Mozambique. Remote Sens. 12, 1279. https://doi.org/10.3390/rs12081279.
Marengo, J.A., Nobre, C.A., Tomasella, J., Oyama, M.D., Sampaio de Oliveira, G., de Oliveira, R., Camargo, H., Alves, L.M., Brown, I.F., 2008. The drought of Amazonia in 2005. J. Clim. 21, 495–516. https://doi.org/10.1175/2007JCLI1600.1.
Masek, J.G., Vermote, E.F., Saleous, N.E., Wolfe, R., Hall, F.G., Huemmrich, K.F., Gao, F., Kutler, J., Lim, T.-K., 2006. A Landsat surface reflectance dataset for North America, 1990-2000. IEEE Geosci. Remote Sens. Lett. 3, 68–72. https://doi.org/10.1109/LGRS.2005.857030.
Matricardi, E.A.T., Skole, D.L., Costa, O.B., Pedlowski, M.A., Samek, J.H., Miguel, E.P., 2020. Long-term forest degradation surpasses deforestation in the Brazilian Amazon. Science (80-.) 369. https://doi.org/10.1126/science.abb3021, 1378 LP – 1382.
Mitchell, A.L., Rosenqvist, A., Mora, B., 2017. Current remote sensing approaches to monitoring forest degradation in support of countries measurement, reporting and verification (MRV) systems for REDD+. Carbon Balance Manag. 12, 9. https://doi.org/10.1186/s13021-017-0078-9.
Näschen, K., Diekkrüger, B., Leemhuis, C., Seregina, L., van der Linden, R., 2019. Impact of climate change on water resources in the Kilombero catchment in Tanzania. Water 11, 859. https://doi.org/10.3390/w11040859.
Olofsson, P., Arévalo, P., Espejo, A.B., Green, C., Lindquist, E., McRoberts, R.E., Sanz, M. J., 2020. Mitigating the effects of omission errors on area and area change estimates. Remote Sens. Environ. 236, 111492 https://doi.org/10.1016/j.rse.2019.111492.
Olsson, P.-O., Lindström, J., Eklundh, L., 2016. Near real-time monitoring of insect induced defoliation in subalpine birch forests with MODIS derived NDVI. Remote Sens. Environ. 181, 42–53. https://doi.org/10.1016/j.rse.2016.03.040.
Pasquarella, V., Bradley, B., Woodcock, C., 2017. Near-real-time monitoring of insect defoliation using Landsat time series. Forests 8, 275. https://doi.org/10.3390/f8080275.
Pfaff, A.S.P., 1999. What drives deforestation in the Brazilian Amazon?: evidence from satellite and socioeconomic data. J. Environ. Econ. Manag. 37, 26–43. https://doi.org/10.1006/jeem.1998.1056.
Poorter, L., Bongers, F., Aide, T.M., Almeyda Zambrano, A.M., Balvanera, P., Becknell, J. M., Boukili, V., Brancalion, P.H.S., Broadbent, E.N., Chazdon, R.L., Craven, D., de Almeida-Cortez, J.S., Cabral, G.A.L., de Jong, B.H.J., Denslow, J.S., Dent, D.H., DeWalt, S.J., Dupuy, J.M., Durán, S.M., Espírito-Santo, M.M., Fandino, M.C., César, R.G., Hall, J.S., Hernandez-Stefanoni, J.L., Jakovac, C.C., Junqueira, A.B., Kennard, D., Letcher, S.G., Licona, J.-C., Lohbeck, M., Marín-Spiotta, E., Martínez-Ramos, M., Massoca, P., Meave, J.A., Mesquita, R., Mora, F., Muñoz, R., Muscarella, R., Nunes, Y.R.F., Ochoa-Gaona, S., de Oliveira, A.A., Orihuela-Belmonte, E., Peña-Claros, M., Pérez-García, E.A., Piotto, D., Powers, J.S., Rodríguez-Velázquez, J., Romero-Pérez, I.E., Ruíz, J., Saldarriaga, J.G., Sanchez-Azofeifa, A., Schwartz, N.B., Steininger, M.K., Swenson, N.G., Toledo, M., Uriarte, M., van Breugel, M., van der Wal, H., Veloso, M.D.M., Vester, H.F.M., Vicentini, A., Vieira, I. C.G., Bentos, T.V., Williamson, G.B., Rozendaal, D.M.A., 2016. Biomass resilience of neotropical secondary forests. Nature 530, 211–214. https://doi.org/10.1038/nature16512.
Ravikumar, A., Sears, R.R., Cronkleton, P., Menton, M., Pérez-Ojeda del Arco, M., 2017. Is small-scale agriculture really the main driver of deforestation in the Peruvian Amazon? Moving beyond the prevailing narrative. Conserv. Lett. 10, 170–177. https://doi.org/10.1111/conl.12264.
Reid, J.L., Fagan, M.E., Lucas, J., Slaughter, J., Zahawi, R.A., 2019. The ephemerality of secondary forests in southern Costa Rica. Conserv. Lett. 12, e12607 https://doi.org/10.1111/conl.12607.
Rozendaal, D.M.A., Bongers, F., Aide, T.M., Alvarez-Dávila, E., Ascarrunz, N., Balvanera, P., Becknell, J.M., Bentos, T.V., Brancalion, P.H.S., Cabral, G.A.L., Calvo-Rodriguez, S., Chave, J., César, R.G., Chazdon, R.L., Condit, R., Dallinga, J.S., de Almeida-Cortez, J.S., de Jong, B., de Oliveira, A., Denslow, J.S., Dent, D.H., DeWalt, S.J., Dupuy, J.M., Durán, S.M., Dutrieux, L.P., Espírito-Santo, M.M., Fandino, M.C., Fernandes, G.W., Finegan, B., García, H., Gonzalez, N., Moser, V.G., Hall, J.S., Hernández-Stefanoni, J.L., Hubbell, S., Jakovac, C.C., Hernández, A.J., Junqueira, A.B., Kennard, D., Larpin, D., Letcher, S.G., Licona, J.-C., Lebrija-Trejos, E., Marín-Spiotta, E., Martínez-Ramos, M., Massoca, P.E.S., Meave, J.A., Mesquita, R.C.G., Mora, F., Müller, S.C., Muñoz, R., de Oliveira Neto, S.N., Norden, N., Nunes, Y.R.F., Ochoa-Gaona, S., Ortiz-Malavassi, E., Ostertag, R., Peña-Claros, M., Pérez-García, E.A., Piotto, D., Powers, J.S., Aguilar-Cano, J., Rodriguez-Buritica, S., Rodríguez-Velázquez, J., Romero-Romero, M.A., Ruíz, J., Sanchez-Azofeifa, A., de Almeida, A.S., Silver, W.L., Schwartz, N.B., Thomas, W.W., Toledo, M., Uriarte, M., de Sá Sampaio, E.V., van Breugel, M., van der Wal, H., Martins, S.V., Veloso, M.D.M., Vester, H.F.M., Vicentini, A., Vieira, I.C.G., Villa, P., Williamson, G.B., Zanini, K.J., Zimmerman, J., Poorter, L., 2019. Biodiversity recovery of Neotropical secondary forests. Sci. Adv. 5 https://doi.org/10.1126/sciadv.aau3114 eaau3114.
Scullion, J.J., Vogt, K.A., Sienkiewicz, A., Gmur, S.J., Trujillo, C., 2014. Assessing the influence of land-cover change and conflicting land-use authorizations on ecosystem conversion on the forest frontier of Madre de Dios, Peru. Biol. Conserv. 171, 247–258. https://doi.org/10.1016/j.biocon.2014.01.036.
Shimizu, K., Ota, T., Mizoue, N., 2019. Detecting forest changes using dense Landsat 8 and Sentinel-1 time series data in tropical seasonal forests. Remote Sens. https://doi.org/10.3390/rs11161899.

Sills, E.O., Atmadja, S., de Sassi, C., Duchelle, A.E., Kweka, D., Resosudarmo, I.A.P., Sunderlin, W.D., 2014. REDD+ on the Ground: A Case Book of Subnational Initiatives across the Globe. Center for International Forestry Research (CIFOR), Bogor, Indonesia. https://doi.org/10.17528/cifor/005202.

Stehman, S.V., 2014. Estimating area and map accuracy for stratified random sampling when the strata are different from the map classes. Int. J. Remote Sens. 35, 4923–4939. https://doi.org/10.1080/01431161.2014.930207.

Stehman, S.V., Wickham, J.D., Smith, J.H., Yang, L., 2003. Thematic accuracy of the 1992 National Land-Cover Data for the eastern United States: statistical methodology and regional results. Remote Sens. Environ. 86, 500–516. https://doi.org/10.1016/S0034-4257(03)00128-7.

Tyukavina, A., Stehman, S.V., Potapov, P.V., Turubanova, S.A., Baccini, A., Goetz, S.J., Laporte, N.T., Houghton, R.A., Hansen, M.C., 2013. National-scale estimation of gross forest aboveground carbon loss: a case study of the Democratic Republic of the Congo. Environ. Res. Lett. 8, 44039. https://doi.org/10.1088/1748-9326/8/4/044039.

Vancutsem, C., Achard, F., Pekel, J.-F., Vieilledent, G., Carboni, S., Simonetti, D., Gallego, J., Aragao, L., Nasi, R., 2020. Long-term (1990-2019) monitoring of tropical moist forests dynamics. bioRxiv 2020.09.17.295774. https://doi.org/10.1101/2020.09.17.295774.

Verbesselt, J., Hyndman, R., Zeileis, A., Culvenor, D., 2010. Phenological change detection while accounting for abrupt and gradual trends in satellite image time series. Remote Sens. Environ. 114, 2970–2980. https://doi.org/10.1016/j.rse.2010.08.003.

Verbesselt, J., Zeileis, A., Herold, M., 2012. Near real-time disturbance detection using satellite image time series. Remote Sens. Environ. 123, 98–108. https://doi.org/10.1016/j.rse.2012.02.022.

Vermote, E., Justice, C., Claverie, M., Franch, B., 2016. Preliminary analysis of the performance of the Landsat 8/OLI land surface reflectance product. Remote Sens. Environ. 185, 46–56. https://doi.org/10.1016/j.rse.2016.04.008.

Wand, M.P., Jones, C., 1994. Multivariate plug-in bandwidth selection. Comput. Stat. 9, 97–116.

Wessel, M., Quist-Wessel, P.M.F., 2015. Cocoa production in West Africa, a review and analysis of recent developments. NJAS - Wageningen J. Life Sci. 74–75, 1–7. https://doi.org/10.1016/j.njas.2015.09.001.

Wulder, M.A., Masek, J.G., Cohen, W.B., Loveland, T.R., Woodcock, C.E., 2012. Opening the archive: how free data has enabled the science and monitoring promise of Landsat. Remote Sens. Environ. 122, 2–10. https://doi.org/10.1016/j.rse.2012.01.010.

Zhu, Z., Woodcock, C.E., 2014. Continuous change detection and classification of land cover using all available Landsat data. Remote Sens. Environ. 144, 152–171. https://doi.org/10.1016/j.rse.2014.01.011.

Zhu, Z., Woodcock, C.E., Olofsson, P., 2012. Continuous monitoring of forest disturbance using all available Landsat imagery. Remote Sens. Environ. 122, 75–91. https://doi.org/10.1016/j.rse.2011.10.030.